ACS OMEGA

http://pubs.acs.org/journal/acsodf

Article

Effect of DNA Flexibility on Complex Formation of a Cationic Nanoparticle with Double-Stranded DNA

Sehui Bae, Inrok Oh, Jejoong Yoo, and Jun Soo Kim*

Cite This: *ACS Omega* 2021, 6, 18728−18736

Read Online

ACCESS | Metrics & More | Article Recommendations | Supporting Information

ABSTRACT: We present extensive molecular dynamics simulations of a cationic nanoparticle and a double-stranded DNA molecule to discuss the effect of DNA flexibility on the complex formation of a cationic nanoparticle with double-stranded DNA. Martini coarse-grained models were employed to describe double-stranded DNA molecules with two different flexibilities and cationic nanoparticles with three different electric charges. As the electric charge of a cationic nanoparticle increases, the degree of DNA bending increases, eventually leading to the wrapping of DNA around the nanoparticle at high electric charges. However, a small increase in the persistence length of DNA by 10 nm requires a cationic nanoparticle with a markedly increased electric charge to bend and wrap DNA around. Thus, a more flexible DNA molecule bends and wraps around a cationic nanoparticle with an intermediate electric charge, whereas a less flexible DNA molecule binds to a nanoparticle with the same electric charge without notable bending. This work provides solid evidence that a small difference in DNA flexibility (as small as 10 nm in persistence length) has a substantial influence on the complex formation of DNA with proteins from a biological perspective and suggests that the variation of sequence-dependent DNA flexibility can be utilized in DNA nanotechnology as a new tool to manipulate the structure of DNA molecules mediated by nanoparticle binding.

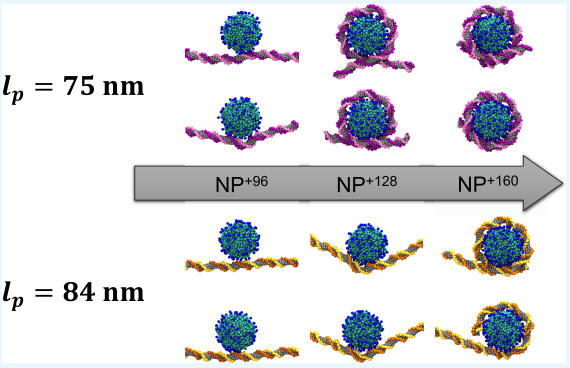

INTRODUCTION

Double-stranded DNA is a rigid polymer chain with an average persistence length (l_p, a measure of rigidity or inverse flexibility) of 50 nm,[1−3] and the local l_p varies by combinations of nucleotides.[4−6] For instance, the local l_p of pairs of consecutive nucleotides (called dinucleotide steps) ranges between 40.9 and 56.0 nm.[4] However, the sequence-dependent variation in DNA flexibility has a negligible effect on the structure of bare DNA molecules. The theory of elastic rods predicts that the effect of DNA flexibility variation is significant when DNA is bent abruptly into an arc with a radius of several nanometers.[3] Therefore, sequence-dependent variation in DNA flexibility is particularly important in biology, where a DNA double helix is bound to and wrapped 1.7 turns around a histone protein complex, forming nucleosomes with a cylindrical shape of 11 nm in diameter and 5.5 nm in height.[2]

Cationic nanoparticles (NPs) with a diameter of several nanometers have been used to mimic histone protein complexes: cationic NPs bind noncovalently to negatively charged DNA, and DNA bends and wraps around cationic NPs, promoting DNA compaction.[7−10] Cationic NPs have also been used as a transfection agent to deliver DNA into cells in biotechnological applications.[11−15] Understanding the effect of DNA flexibility on complex formation with cationic NPs will further help the development of biotechnological applications.[16]

Here, we used extensive molecular dynamics (MD) simulations of Martini coarse-grained (CG) models of a cationic NP and a double-stranded DNA molecule to investigate the effect of DNA flexibility on the formation of DNA−NP complexes. Two DNA sequences with 100 base pairs (bp) of $(AT)_{50}/(AT)_{50}$ and $(AC)_{50}/(GT)_{50}$ were chosen to represent more and less flexible DNA fragments, respectively, with l_p differing by 10 nm. A cationic NP with 7 nm in diameter was chosen as a mimic of the histone protein complex to induce abrupt bending and wrapping of DNA. In this paper, DNA refers to double-stranded DNA molecules, and DNA length in bp refers to the number of constituting pairs of complementary bases or nucleotides.

Computer simulations have been used to investigate the binding of double-stranded DNA with various associating molecules, including proteins, NPs, dendrimers, and polyamines.[16−39] Albeit invaluable, MD simulations based on all-atom models[17−26] are time-consuming and computationally

Received: March 30, 2021
Accepted: July 5, 2021
Published: July 15, 2021

expensive. Therefore, the length of DNA fragments considered in MD simulations is typically no longer than 50 bps, which is too short to facilitate bending and wrapping around a cationic NP, except for a few examples.[26] Although there have been several atomistic MD simulations employing DNA fragments of ∼150 bps,[27−30] these studies focused on the stability and structural features of nucleosomes (in which the DNA fragment is already wrapped around the histone protein complex) but not on the dynamic process of DNA binding and wrapping. The use of CG models[40−45] can be an alternative to investigate complex formation between DNA and binding molecules by enabling relatively longer and larger scales of MD simulations.[16,31−39] However, depending on the coarse-graining philosophy, CG models have lists of specific features to determine the model most appropriate to answer specific questions. Among several CG models of DNA, the Martini DNA model is chosen in this work to investigate the effect of DNA flexibility on the complex formation of a cationic NP and a DNA fragment. This model has sequence specificity for flexibility variation, and many details, including solvents and ions, are explicitly implemented to describe the molecular interactions better.[43]

Simulation results show that DNA flexibility determines the structure of a complex formed between a cationic NP and a DNA fragment. As the electric charge of a cationic NP increases, the degree of DNA bending increases and, eventually, DNA wraps around the NP at high electric charges. However, a decrease in DNA flexibility due to a 10 nm increase in l_p requires a marked increase in the electric charge of a cationic NP for DNA bending and wrapping around the NP. As a result, for an intermediate electric charge, the more flexible DNA fragment bends and wraps around the NP, whereas the less flexible DNA fragment binds to the NP without notable bending.

The rest of this paper is organized as follows. We describe the simulation model and method in the following section. Simulation results are presented in the section "Results and Discussion", where we compare the complex formation of a cationic NP with two DNA sequences of different flexibilities and discuss the consequences of DNA flexibility on NP-induced DNA compaction. This work is summarized in the section "Conclusions".

METHODS

Martini CG Models of DNA and NP. We used the Martini CG models developed by Marrink and co-workers[43,47] and its adaptation for the NP,[48] as shown in Figure 1. All-atom models of DNA molecules were generated by the Nucleic Acid Builder (NAB) program in AmberTools16,[49] and were transformed into Martini CG models of DNA by the Python script provided by Marrink and co-workers.[43,50] Each nucleotide is mapped to six or seven CG beads. Three beads represent the backbone consisting of a phosphate group and a sugar moiety, and the remaining three or four beads represent a pyrimidine or purine base, respectively. The overall particle types and parameters[43] are listed in Tables S1−S3 of the Supporting Information. In particular, the structure of the double-stranded DNA is maintained by the soft elastic network model, in which a harmonic force is applied between the backbone beads and between a backbone bead and the first connected bead in each base.[43]

To model a cationic NP, its core structure was built by face-centered cubic packing of gold (Au) beads in a truncated octahedron with a dimension of ∼4 nm between the two opposite faces. Au beads were restrained by the harmonic potential among each other. On the surface of the Au core, 296 octanethiol ligands were attached so that the ligand footprint of 20.6 Å^2 was close to 21.6 Å^2, which is the experimental value.[51] Among them, 96, 128, and 160 ligands were functionalized by a cationic end to model the cationic NPs with electric charges of +96e, +128e, and +160e, respectively, where e is the elementary charge. Octanethiol ligands were modeled by four or five beads for neutral or cationic ligands, and one end of each ligand was restrained on the surface of the Au core by a harmonic potential. The diameter of the ligand-stabilized NP was estimated to be ∼7 nm, as shown by the radial distribution function in Figure S1(A) of the Supporting Information. The overall particle types and parameters of the NP are listed in Table S4 of the Supporting Information.

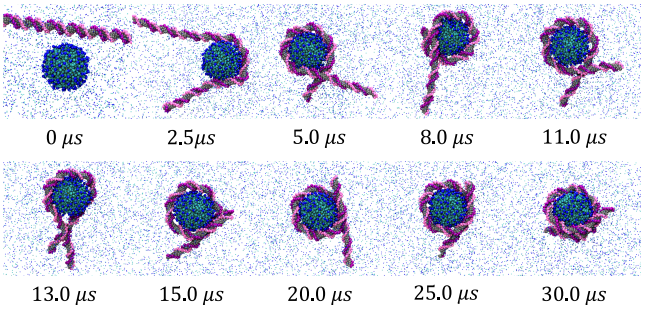

Figure 1. Simulation snapshots showing time-dependent DNA binding and wrapping around a cationic NP. The DNA fragment is 100-bp-long with a sequence of $(AT)_{50}/(AT)_{50}$. The cationic NP has an electric charge of +160e. DNA backbone groups are colored in violet and magenta, DNA bases in gray, cationic end groups of the NP in blue, and neutral ligands on the NP in cyan. Na^+ and Cl^- ions are shown as points in the background, and water molecules are hidden for ease of visualization. Images were generated using VMD.[46]

The l_p of the Martini DNA model was estimated by separate MD simulations of a linear DNA molecule. DNA bond vectors were defined as the distance between the centers-of-mass of two consecutive pairs of complementary nucleotides, and the average orientational correlation was calculated as

$$\langle \vec{b}_i \cdot \vec{b}_j \rangle = b^2 \exp(-b|i-j|/l_p) \quad (1)$$

where $\vec{b}_i$ and $\vec{b}_j$ are the ith and jth bond vectors, respectively; b is the average bond length; and $\langle \cdots \rangle$ is the average overall DNA conformations at equilibrium. By fitting the data to the exponential function of eq 1, l_p was obtained as 75 and 84 nm for $(AT)_{50}/(AT)_{50}$ and $(AC)_{50}/(GT)_{50}$, respectively, as shown in Figure 2.

MD Simulations for Complex Formation. To investigate complex formation between a 100-bp-long DNA and a cationic NP, the models of DNA and the NP were placed in a rhombic dodecahedron box with a lattice length of 36.3 nm and solvated with Martini water particles. Initially, the NP was placed 1.5 nm from the central region of DNA. Ten percent of the water particles were replaced by Martini antifreeze particles. Na^+ and Cl^- ions were added to set the concentration at 0.150 M, and additional Na^+ ions were added for the charge neutralization. For instance, for the system with an NP with +160e, the numbers of Na^+ and Cl^- ions were 3092 and 3054, respectively, in the system volume of 33 800 nm^3, corresponding to the ion concentrations of 0.152 and 0.150 M for Na^+

https://doi.org/10.1021/acsomega.1c01709
ACS Omega 2021, 6, 18728−18736

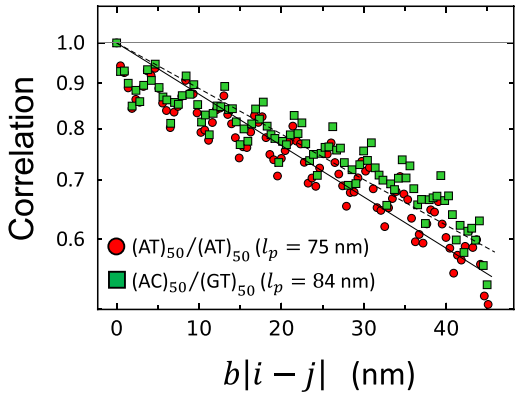

Figure 2. Correlation functions of DNA bond vectors were calculated as a function of bond separation, $b|i-j|$, as expressed in eq 1, where b is an average bond length and i and j are index numbers of the bond vectors. The correlation functions were fitted to exponential functions (dashed and solid curves), resulting in l_p of 75 and 84 nm for sequences of $(AT)_{50}/(AT)_{50}$ and $(AC)_{50}/(GT)_{50}$, respectively.

and Cl^- ions, respectively. The system was energy minimized and equilibrated in constant NVT and NPT conditions. During the NPT equilibration to keep the pressure constant at 1 bar, the system volume increased and the ion concentrations were slightly reduced to 0.143 and 0.142 M for Na^+ and Cl^- ions. The production simulation was performed for a duration of 10 μs for all sets. In the case of significant DNA bending, the production simulation was extended for another 20 μs. All of the MD simulations were performed using the GROMACS 2019 package.[52] The integration time step was 10 fs. The temperature was set to 300 K using a velocity rescaling thermostat, and the pressure was set to 1 bar using the Berendsen barostat. A cutoff of 1.1 nm was used for van der Waals interactions. A reaction field method was used to treat Coulomb interactions with a cutoff at 1.1 nm. Relative dielectric constants for the medium and the reaction field were set to 15 and infinity, respectively.[53,54]

RESULTS AND DISCUSSION

We performed extensive MD simulations of a 100-bp-long DNA fragment and a cationic NP of 7.0 nm in diameter using Martini CG models. To explore the influence of DNA persistence length (l_p) on complex formation with a cationic NP, we considered two DNA fragments with l_p that differ by 10 nm: a more flexible fragment of $(AT)_{50}/(AT)_{50}$ with an average l_p of 75 nm and a less flexible fragment of $(AC)_{50}/(GT)_{50}$ with an average l_p of 84 nm. Due to the overestimation of the l_p of these DNA models by about 30 nm compared with an average DNA l_p of 50 nm, we focused on the qualitative

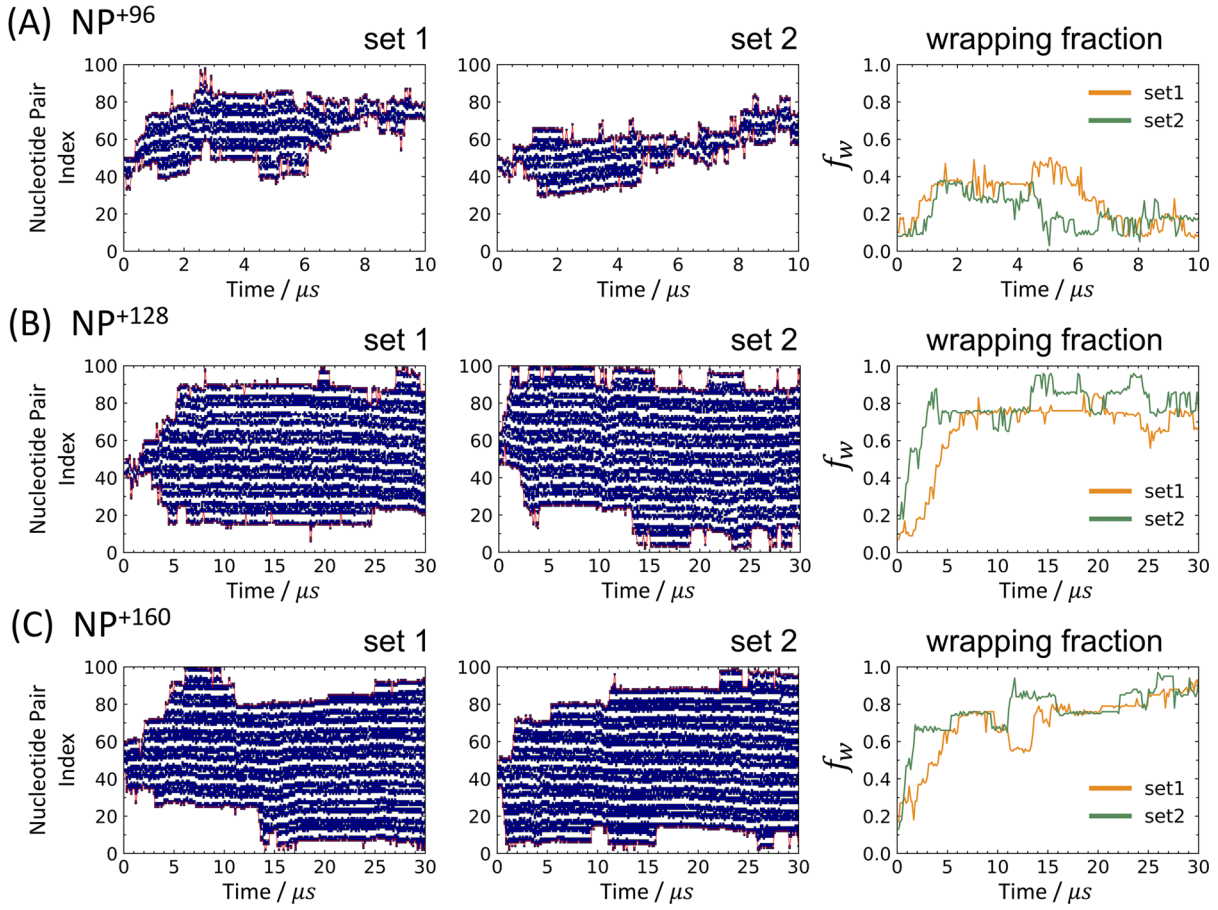

Figure 3. Binding of $(AT)_{50}/(AT)_{50}$ to cationic NPs with electric charges of (A) +96e, (B) +128e, and (C) +160e. The first two columns present two independent sets of simulation data showing the time evolution of DNA contacts with an NP. Filled symbols in dark blue indicate the indices of nucleotide pairs (or the regions of DNA) bound to the NP. Red lines on top and bottom indicate boundaries between the bent and linear regions of DNA, and their difference defines the fraction of DNA wrapping, f_w. The last column presents the variation of f_w with time for the two simulation sets.

https://doi.org/10.1021/acsomega.1c01709
ACS Omega 2021, 6, 18728−18736

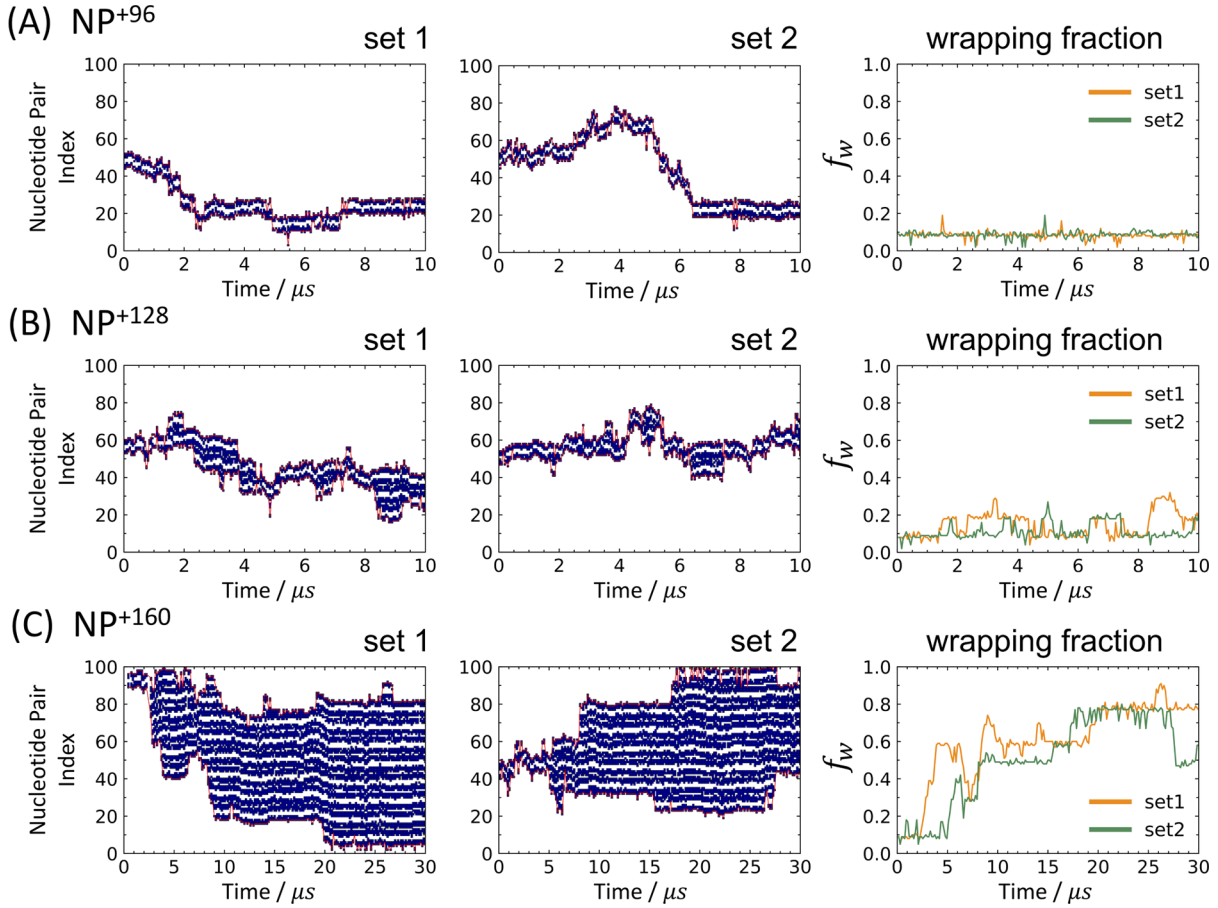

Figure 4. Binding of $(AC)_{50}/(GT)_{50}$ to cationic NPs with electric charges of (A) +96e, (B) +128e, and (C) +160e. The first two columns present two independent sets of simulation data showing the time evolution of DNA contacts with an NP. Filled (dark blue) symbols indicate the indices of nucleotide pairs (or the regions of DNA) bound to the NP. Red lines on top and bottom indicate boundaries between the bent and linear regions of DNA, and their difference defines the fraction of DNA wrapping, f_w. The last column presents the variation of f_w with time for the two simulation sets.

difference of DNA−NP binding arising from a 10 nm difference in l_p. This difference is close to that predicted using the local l_p of dinucleotide steps of AT/AT and AC/GT reported previously.[4] An NP with a diameter of 7.0 nm is a mimic of the histone protein complex, and it induces abrupt DNA bending for sufficiently high electric charges of an NP. Although the 100-bp-long DNA fragments have a fixed charge of −198e (two phosphates with −1e per pair of complementary nucleotides except the nucleotides at each 5' end), three values of electric charge of an NP of +96e, +128e, and +160e were considered. For each set of two DNA flexibilities and three NP charges, two independent sets of simulations were performed to confirm the results, a total of 12 sets of extensive MD simulations. We performed 10-μs-long simulations for all simulation sets. Those with significant DNA bending were extended to 30 μs to investigate how the DNA wraps around an NP.

Simulation results are presented in Figure 1 for a DNA fragment of $(AT)_{50}/(AT)_{50}$ and a cationic NP with a charge of +160e. The electric charge of the NP is high enough to induce complete wrapping of the DNA fragment around the NP. The figure presents simulation snapshots taken at various times to monitor the binding and wrapping of the DNA fragment around the NP. Initially, the DNA is placed 1.5 nm from a cationic NP. With time, the negatively charged DNA fragment and the cationic NP bind to each other due to electrostatic attraction. At 2.5 μs, the DNA fragment is bent around the NP and makes a complete turn at 5.0 μs. Two flanking ends of the DNA fragment take turns binding to and dissociating from the surface of the NP, resulting in translational movement (or sliding) of the NP along the DNA fragment. The NP was located at the center of the DNA fragment at 5.0 and 11.0 μs, whereas the NP was found at each end of the DNA fragment at 8.0 and 15.0 μs. Finally, the two flanking ends bind to the NP, completing the DNA wrap, as shown at 30.0 μs in the figure.

The process of DNA binding and wrapping is presented in more detail in terms of the time evolution of DNA contacts with an NP, as shown in Figures 3 and 4 for DNA fragments of $(AT)_{50}/(AT)_{50}$ and $(AC)_{50}/(GT)_{50}$, respectively. A pair of complementary nucleotides of a DNA fragment is considered bound to the NP when any of the two negatively charged particles (representing the phosphates) of the nucleotide pair is within a distance of 0.7 nm from any positively charged particle of the cationic ligand on the NP. The critical distance of 0.7 nm is chosen based on the first minimum of the radial distribution function between them, as shown in Figure S1(B) of the Supporting Information. In Figures 3 and 4, the nucleotide pairs bound to the NP are indicated as filled symbols.

At each time in the figures, about six filled symbols appear together next to each other along the vertical direction, indicating that phosphates of six proximal nucleotide pairs bind

https://doi.org/10.1021/acsomega.1c01709
ACS Omega 2021, 6, 18728−18736

to cationic ligands of the NP at the same time. In addition, groups of the six binding nucleotide pairs are shown discretely and periodically along the DNA (or along the vertical axis) with an average increase of 9.6 (±0.0) nucleotide pairs. This periodicity of the binding groups originates from the helical structure of DNA (with the number of nucleotide pairs of 9.6 per helical turn being slightly different from 10.5 bps of B-DNA, ascribed to the approximate nature of the CG model of DNA). In the DNA model, several phosphates in every 9.6 nucleotide pairs face the NP, whereas the others turn away from the NP. As a result, about six nucleotide pairs bind together to the NP in each helical turn, while the nucleotide pairs located between the binding groups of six nucleotide pairs are not in direct contact with cationic ligands. However, these in-between nucleotide pairs are still a part of the DNA structure wrapping around the NP. Therefore, we define the DNA wrapping fraction, f_w, as the fraction of DNA nucleotide pairs bent close to the NP, which includes both binding and in-between nucleotide pairs. The variable f_w is practically calculated by the difference between the top and bottom of the filled symbols, as bounded by solid red lines in the figures. The time-dependent variation of f_w is presented in the last column of Figures 3 and 4.

It is evident in Figures 3 and 4 that as the electric charge of a cationic NP increases from +96e to +160e, f_w increases. Given the small surface area of an NP with a diameter of 7 nm, the variation of f_w indicates the structural transition from a linear DNA with marginal bending at low electric charges to a bent DNA structure wrapping around the NP at high electric charges. Since the common form of DNA (B-DNA) has a diameter of 2.0 nm and a rise per base pair of 0.33 nm, a single turn of DNA around an NP with a diameter of 7 nm requires, theoretically, 83 base pairs to be in contact with the NP. Therefore, the value of f_w close to 0.8 indicates, roughly, a complete turn of DNA around the NP.

In the case of $(AT)_{50}/(AT)_{50}$ shown in Figure 3, the transition from linear to wrapped DNA structures occurs between +96e and +128e. At a low electric charge of +96e, DNA quickly binds to the NP, and with time, up to five and six helical turns of DNA bind with the NP. However, DNA binding and unbinding are reversible and at the end of the simulations, the number of DNA contacts decreases to a few DNA helical turns, suggesting that DNA binds with the NP with marginal DNA bending. On the contrary, at the electric charges of +128e and +160e, the electrostatic attraction between the DNA and the NP is strong enough to wrap DNA around the NP, as shown by a large number of DNA contacts with an NP and the significant fraction of DNA wrapping.

The variation of DNA contacts shown in "set 1" of Figure 3(C) corresponds to the simulation snapshots presented in Figure 1 and is noteworthy because it reveals the structural fluctuations in the course of DNA wrapping. At the beginning of the simulation, DNA binds quickly to the NP in the central region of the DNA fragment. As time increases to 6.0 μs, one flanking end of the DNA fragment progressively binds to the NP and maintains the wrapping structure for another 4.0 μs. However, at 10.0 μs, the DNA end separates from the NP; at 13.0 μs, the other flanking end of the DNA fragment starts to bind to the NP. The bent structure of this DNA end remains stable until the end of the simulation, and the DNA wrapping is completed at 25.0 μs. The structural fluctuations by sequential binding and unbinding of the two flanking ends indicate the translational movement or sliding motion of the NP along the DNA fragment, as discussed above based on the simulation snapshots of Figure 1.

In the case of $(AC)_{50}/(GT)_{50}$ shown in Figure 4, the transition from linear to wrapped DNA structures occurs between +128e and +160e. At low electric charges of +96e and +128e, DNA quickly binds to the NP. However, the number of DNA contacts never grows more than a couple of DNA helical turns. This fragment is slightly less flexible because of the 10 nm increase in l_p than $(AT)_{50}/(AT)_{50}$, and its effect on complex formation is sufficiently large. This DNA fragment rarely bends upon binding to the cationic NP with electric charges of +96e and +128e. When the electric charge is increased to +160e, the number of DNA contacts and the value of f_w increase significantly with time, suggesting significant bending and wrapping of DNA. It is noteworthy that a 10 nm increase in the l_p of DNA from $(AT)_{50}/(AT)_{50}$ to $(AC)_{50}/(GT)_{50}$ requires a much higher electric charge of a cationic NP for DNA to bend and wrap around the NP. As a result, the more flexible fragment of $(AT)_{50}/(AT)_{50}$ bends and wraps around the NP at an intermediate electric charge of +128e, whereas the less flexible fragment of $(AC)_{50}/(GT)_{50}$ binds to the NP of the same electric charge without significant bending.

The difference in DNA−NP binding for $(AT)_{50}/(AT)_{50}$ and $(AC)_{50}/(GT)_{50}$ can be attributed most clearly to the different elastic energy of DNA bending. According to the theory of elastic rods, bending of DNA with length L requires an amount of energy $\xi k_B TL/R^2$ to induce DNA deformation into an arc with radius R, where k_B is the Boltzmann constant, T is the absolute temperature, and ξ is the persistence length.[3] The average length of each base pair of the Martini CG model in our simulations was estimated to be 0.41 nm/bp, and the radius of the DNA wrap in Figure 1 was estimated to be 4.5 nm. Using ξ = 75 and 84 for $(AT)_{50}/(AT)_{50}$ and $(AC)_{50}/(GT)_{50}$, the energy of DNA bending is estimated for a single turn of DNA around an NP at 300 K to be 263 kJ/mol (= $105k_BT$) and 293 kJ/mol (= $117k_BT$), respectively, with a difference of 30 kJ/mol. These approximate estimates of DNA bending energy explain the qualitative difference of DNA−NP binding for $(AT)_{50}/(AT)_{50}$ and $(AC)_{50}/(GT)_{50}$.

Beyond this simple picture of DNA as an elastic rod, ionic environments around negatively and positively charged DNA and the NP play critical roles in determining the complex formation between the DNA and the NP. The role of counterions has been of particular interest to elucidate the DNA condensation into toroids and rods in the presence of multivalent ions. Counterions condense onto DNA, and in the case of multivalent ions, strong electrostatic repulsions between DNA phosphates are overcome to lead to the DNA condensation.[55−57] To confirm the localization of counterions near DNA and the NP, we calculated the radial distribution functions between DNA phosphates and Na^+ ions and between NP cationic ligands and Cl^-, as presented in Figure S2 of the Supporting Information. The first peaks of the radial distribution functions are well defined with large values, suggesting that the counterions, Na^+ and Cl^-, are highly concentrated near DNA and the NP, respectively. The binding of the counterions to DNA reduces strong repulsions between DNA phosphates and increased the flexibility of DNA, facilitating DNA bending around the NP. In addition to the local condensation of Na^+ ions to DNA, asymmetric charge neutralization of DNA induced by binding of a positively charged NP can also facilitate DNA bending and thus the complex formation between the DNA and the NP. The

https://doi.org/10.1021/acsomega.1c01709
ACS Omega 2021, 6, 18728−18736

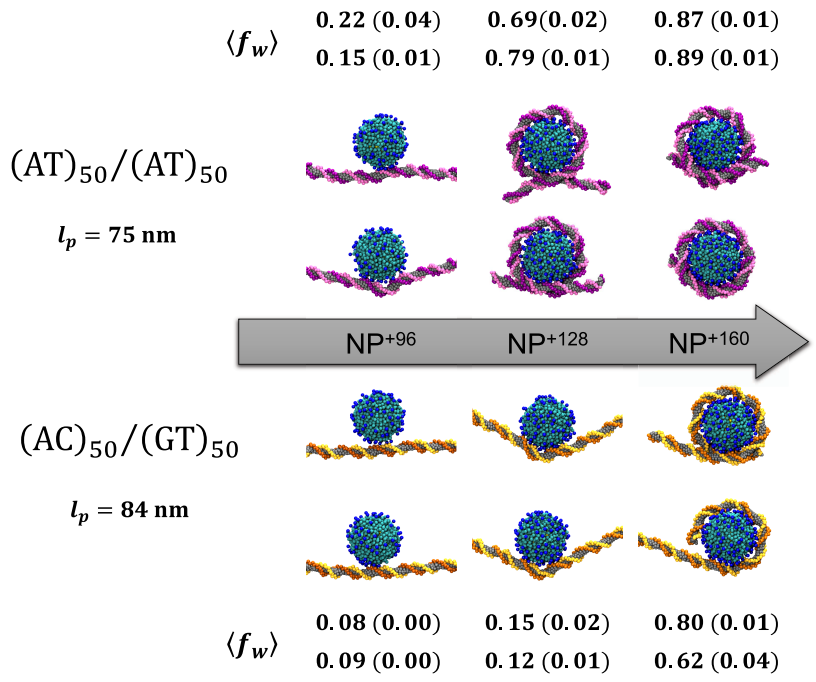

Figure 5. Final snapshots from the MD simulations of binding between a 100-bp-long DNA fragment and a cationic NP. Comparisons among simulations with a cationic NP with varying electric charges of +96e, +128e, and +160e and with two DNA fragments of $(AT)_{50}/(AT)_{50}$ and $(AC)_{50}/(GT)_{50}$. $\langle f_w \rangle$ is the average value of the DNA wrapping fraction, f_w, presented in Figures 3 and 4 over the last 5 μs of each simulation. The values in the parentheses are the error estimates calculated by the batch-means method. Color codes are the same as in Figure 1, except for those of DNA backbone groups for $(AC)_{50}/(GT)_{50}$ in orange and yellow. The images were generated using VMD.[46]

asymmetric charge neutralization on one side of the DNA close to the NP results in unbalanced repulsive forces of DNA phosphates between the neutralized and repulsive sides of the DNA and facilitates the preferential DNA bending toward the NP.[58−60]

In Figure 4, it is also noteworthy that a cationic NP does not remain static on DNA,[16,39] in particular, at low electric charges of an NP with which DNA is not bent significantly. At +96e and +128e, the index numbers of nucleotide pairs in contact with an NP fluctuate with time, indicating the movement of the NP along DNA. In principle, NP movement can occur in two different mechanisms along DNA: either an NP moves helically along DNA grooves with a coupling between translational and rotational motions or an NP moves straight along DNA by stepping across major and minor grooves. The coupling of translational motion with helical rotation along DNA has been suggested for DNA-binding proteins.[61] In our analysis of the time evolution of DNA−NP contacts, such coupling between translation and rotation would result in continuous variation of DNA−NP contacts without any jump. The figures for +96e and +128e show that the movements of an NP occur in a mixed manner. On large scales, sudden jumps between different DNA helical turns are observed, suggesting that the NP rolls along DNA by stepping across major and minor grooves. However, the coupled movement of translation and rotation is also observed locally by continuous variation of DNA−NP contacts, for instance, between 3.2 and 3.7 μs of "set 2" in Figure 4A.

In summary, the simulation results for 12 sets of extensive MD simulations are summarized in Figure 5. Average values of the wrapping fraction of DNA, $\langle f_w \rangle$, calculated over the final 5 μs of each simulation trajectory, are presented together with the final simulation snapshots. The values in the parentheses are the statistical errors estimated by the batch-means method.

For both DNA fragments, the degree of bending increases as the electric charge of an NP increases from +96e to +128e and to +160e, as indicated by the increase in $\langle f_w \rangle$ as well as by the change in DNA configurations of the final snapshots. At high electric charges, DNA bends and wraps around an NP, and $\langle f_w \rangle$ increases significantly. In the figure, the sudden increase in $\langle f_w \rangle$ accompanying DNA wrapping is observed at different NP charges. For the more flexible $(AT)_{50}/(AT)_{50}$, $\langle f_w \rangle$ suddenly increases between +96e and +128e, whereas for the less flexible $(AC)_{50}/(GT)_{50}$, $\langle f_w \rangle$ increases between +128e and +160e. This suggests that DNA bending and wrapping around a cationic NP are more effective with the more flexible fragment $(AT)_{50}/(AT)_{50}$ than with the less flexible fragment $(AC)_{50}/(GT)_{50}$.

The effect of DNA flexibility can be compared for the same NPs. For the same electric charge of an NP, $\langle f_w \rangle$ is always larger for the more flexible DNA fragment of $(AT)_{50}/(AT)_{50}$ than for the less flexible $(AC)_{50}/(GT)_{50}$. The difference in $\langle f_w \rangle$ is largest for an NP with an electric charge of +128e, suggesting that the more flexible $(AT)_{50}/(AT)_{50}$ bends and wraps around the NP, whereas the less flexible $(AC)_{50}/(GT)_{50}$ binds to the NP without significant bending. This result is particularly interesting because only one of the DNA fragments can bend and wrap around an NP. Thus, introducing a cationic NP with +128e would result in a dramatic difference in DNA conformations in a mixed solution of DNA molecules with different flexibilities.

Finally, we investigated the effect of ion concentration on the stability of a DNA−NP complex, as presented in Figure 6. Previously, we proposed a novel DNA-based Brownian ratchet, by which cationic NPs can be moved in a specific direction along DNA, using Brownian dynamics simulations of a semiflexible polymer model of double-stranded DNA and a spherical model of NP.[16,39] The success of the proposed

https://doi.org/10.1021/acsomega.1c01709
ACS Omega 2021, 6, 18728−18736

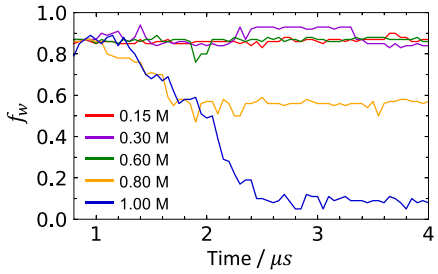

Figure 6. Effect of ion concentration on the stability of a DNA−NP complex. Starting from a DNA−NP complex with DNA of $(AT)_{50}/(AT)_{50}$ around a cationic NP with +160e, the variation of wrapping fraction, f_w, was calculated over time at different concentrations of Na^+ and Cl^- ions.

Brownian ratchet relies on the modulation of DNA−NP binding at different ion concentrations, which was described implicitly by the screened Coulomb potential energy of the Debye−Hückel approximation[62] but not by the explicit presence of ions. Therein, electrostatic interactions between the charged particles were screened out at large separations, as expressed mathematically by an exponential decrease of the potential energy, and more effectively at higher ion concentrations. Here, this assumption of the electrostatic screening is tested explicitly by varying numbers of ions to the solution of a DNA−NP complex.

A final conformation of the DNA−NP complex between $(AT)_{50}/(AT)_{50}$ and a NP with +160e, presented in Figure 5, was prepared with the number of Na^+ and Cl^- ions at each corresponding ion concentration. MD simulations were run for 4 μs, during which the wrapping fraction, f_w, of DNA around the NP was calculated over time. Figure 6 presents the variation of f_w with time at ion concentrations of 0.15, 0.30, 0.60, 0.80, and 1.00 M, and it reveals that the DNA−NP complex remains stable at ion concentrations $\leq$0.60 M, whereas DNA unwraps the NP at higher ion concentrations of 0.80 and 1.00 M. The change in the stability of DNA−NP complexes at high ion concentrations is attributed to the effect of electrostatic screening on the Coulombic attraction between negatively and positively charged moieties of DNA and the NP as well as the stiffness or persistence length of double-stranded DNA. This proves that DNA−NP binding can be modulated by changing the ion concentration in solutions.

CONCLUSIONS

The effect of sequence-dependent variation in DNA flexibility on the structure of bare DNA molecules is negligible. Here, we showed that its effect becomes significant when DNA is bent around a particle with a size of several nanometers. Using the Martini CG models of DNA and NP, we performed MD simulations of the complex formation of a cationic NP and two double-stranded DNA molecules with different flexibilities. As the electric charge of a cationic NP increases, the degree of DNA bending increases and, eventually, DNA wraps around the NP at high NP charges. However, the structures of DNA−NP complexes are significantly influenced by DNA flexibility. For instance, for an NP with an intermediate electric charge, the more flexible DNA fragment bends and wraps around the NP, whereas the less flexible DNA fragment binds to the NP without significant bending. It suggests that a small difference in DNA flexibility (as small as 10 nm in l_p) has a substantial influence on complex formation with proteins. In addition, the sequence-dependent variation of DNA flexibility can be utilized in DNA nanotechnology as a new tool to manipulate the structure of DNA molecules through selective binding with cationic NPs.[16,39] Nevertheless, the results do not provide any conclusions about the thermodynamic preference of the NP binding to two DNA fragments with different flexibilities. Thus, our future research will be to calculate the potential of mean force for DNA wrapping.

In this work, we mainly focused on the role of elastic DNA bending by emphasizing the effect of a small difference in persistence length on complex formation with a cationic NP. However, the complex formation between the DNA and the NP can be attributed to several thermodynamic contributions, in addition to the elastic bending energy of DNA: the electrostatic attraction between the DNA and the NP and with counterions, translational entropy of counterions, and conformational entropy of DNA. Understanding the thermodynamic contributions to the complex formation between the DNA and the NP represents the possible future direction of this work.

The application of Martini CG models enabled longer simulations of larger systems to investigate the process of DNA binding and wrapping around a cationic NP. However, the models are inherently approximate and do not incorporate many details that play important roles in determining the structure and dynamics of double-stranded DNA molecules. For instance, by applying the harmonic potential in the elastic network model to keep the pairs of complementary nucleotides together, the possible formation of kinks by abrupt DNA bending is ignored. Given that atomistic models are too expensive to simulate DNA binding and wrapping around an NP, further refinement of the state-of-the-art CG models is required.

ASSOCIATED CONTENT

Supporting Information

The Supporting Information is available free of charge at https://pubs.acs.org/doi/10.1021/acsomega.1c01709.

Parameters of CG models of DNA and the NP and supporting figures of radial distribution functions (PDF)

AUTHOR INFORMATION

Corresponding Author

Jun Soo Kim − *Department of Chemistry and Nanoscience, Ewha Womans University, Seoul 03760, Republic of Korea;* orcid.org/0000-0001-8113-0605; Email: jkim@ewha.ac.kr

Authors

Sehui Bae − *Department of Chemistry and Nanoscience, Ewha Womans University, Seoul 03760, Republic of Korea*

Inrok Oh − *LG Chem Ltd., Seoul 07796, Republic of Korea*

Jejoong Yoo − *Department of Physics, Sungkyunkwan University, Suwon 16419, Republic of Korea;* orcid.org/0000-0001-7120-8464

Complete contact information is available at: https://pubs.acs.org/10.1021/acsomega.1c01709

Notes

The authors declare no competing financial interest.

■ ACKNOWLEDGMENTS

This research was funded by the National Research Foundation of Korea (NRF) under Grant Nos. NRF-2019R1A2C1084414 and NRF-2020R1A5A2019210.

■ REFERENCES

(1) Hagerman, P. J. Flexibility of DNA. *Annu. Rev. Biophys. Biophys. Chem.* **1988**, *17*, 265−286.
(2) Widom, J. Role of DNA Sequence in Nucleosome Stability and Dynamics. *Quart. Rev. Biophys.* **2001**, *34*, 269−324.
(3) Phillips, R.; Kondev, J.; Theriot, J.; Garcia, H. *Physical Biology of the Cell*, 2nd ed.; Garland Science: New York, 2012.
(4) Geggier, S.; Vologodskii, A. Sequence dependence of DNA bending rigidity. *Proc. Natl. Acad. Sci. U.S.A.* **2010**, *107*, 15421−15426.
(5) Chuang, H.-M.; Reifenberger, J. G.; Cao, H.; Dorfman, K. D. Sequence-Dependent Persistence Lengths of Long DNA. *Phys. Rev. Lett.* **2017**, *119*, No. 227802.
(6) Mitchell, J. S.; Glowacki, J.; Grandchamp, A. E.; Manning, R. S.; Maddocks, J. H. Sequence-Dependent Persistence Lengths of DNA. *J. Chem. Theory Comput.* **2017**, *13*, 1539−1555.
(7) Zinchenko, A. A.; Yoshikawa, K.; Baigl, D. Compaction of Single-Chain DNA by Histone-Inspired Nanoparticles. *Phys. Rev. Lett.* **2005**, *95*, No. 228101.
(8) Zinchenko, A. A.; Sakaue, T.; Araki, S.; Yoshikawa, K.; Baigl, D. Single-Chain Compaction of Long Duplex DNA by Cationic Nanoparticles: Modes of Interaction and Comparison with Chromatin. *J. Phys. Chem. B.* **2007**, *111*, 3019−3031.
(9) Carnerero, J. M.; Masuoka, S.; Baba, H.; Yoshikawa, Y.; Prado-Gotor, R.; Yoshikawa, K. Decorating a Single Giant DNA with Gold Nanoparticles. *RSC Adv.* **2018**, *8*, 26571−26579.
(10) Thomas, T. J.; Thomas, T. Collapse of DNA in Packaging and Cellular Transport. *Int. J. Biol. Macromol.* **2018**, *109*, 36−48.
(11) Kneuer, C.; Sameti, M.; Bakowsky, U.; Schiestel, T.; Schirra, H.; Schmidt, H.; Lehr, C.-M. A Nonviral DNA Delivery System Based on Surface Modified Silica-Nanoparticles Can Efficiently Transfect Cells in Vitro. *Bioconjugate Chem.* **2000**, *11*, 926−932.
(12) Sandhu, K. K.; McIntosh, C. M.; Simard, J. M.; Smith, S. W.; Rotello, V. M. Gold Nanoparticle-Mediated Transfection of Mammalian Cells. *Bioconjugate Chem.* **2002**, *13*, 3−6.
(13) Thomas, M.; Klibanov, A. M. Conjugation to Gold Nanoparticles Enhances Polyethylenimine's Transfer of Plasmid DNA into Mammalian Cells. *Proc. Natl. Acad. Sci. U.S.A.* **2003**, *100*, 9138−9143.
(14) Han, G.; You, C.-C.; Kim, B.-j.; Turingan, R. S.; Forbes, N. S.; Martin, C. T.; Rotello, V. M. Light-regulated Release of DNA and its Delivery to Nuclei by Means of Photolabile Gold Nanoparticles. *Angew. Chem., Int. Ed.* **2006**, *45*, 3165−3169.
(15) Samanta, A.; Medintz, I. L. Nanoparticles and DNA - a Powerful and Growing Functional Combination in Bionanotechnology. *Nanoscale* **2016**, *8*, 9037−9095.
(16) Park, S.; Song, J.; Kim, J. S. In Silico Construction of a Flexibility-Based DNA Brownian Ratchet for Directional Nanoparticle Delivery. *Sci. Adv.* **2019**, *5*, No. eaav4943.
(17) Pavan, G. M.; Danani, A.; Pricl, S.; Smith, D. K. Modeling the Multivalent Recognition between Dendritic Molecules and DNA: Understanding How Ligand "Sacrifice" and Screening can Enhance Binding. *J. Am. Chem. Soc.* **2009**, *131*, 9686−9694.
(18) Chen, C.; Pettitt, B. M. The Binding Process of a Nonspecific Enzyme with DNA. *Biophys. J.* **2011**, *101*, 1139−1147.
(19) Nandy, B.; Maiti, P. K. DNA Compaction by a Dendrimer. *J. Phys. Chem. B* **2011**, *115*, 217−230.
(20) Railsback, J. G.; Singh, A.; Pearce, R. C.; McKnight, T. E.; Collazo, R.; Sitar, Z.; Yingling, Y. G.; Melechko, A. V. Weakly Charged Cationic Nanoparticles Induce DNA Bending and Strand Separation. *Adv. Mater.* **2012**, *24*, 4261−4265.
(21) Nandy, B.; Maiti, P. K.; Bunker, A. Force Biased Molecular Dynamics Simulation Study of Effect of Dendrimer Generation on Interaction with DNA. *J. Chem. Theory Comput.* **2013**, *9*, 722−729.
(22) Mills, M.; Orr, B. G.; Holl, M. M. B.; Andricioaei, I. Attractive Hydration Forces in DNA−Dendrimer Interactions on the Nanometer Scale. *J. Phys. Chem. B* **2013**, *117*, 973−981.
(23) Nash, J. A.; Singh, A.; Li, N. K.; Yingling, Y. G. Characterization of Nucleic Acid Compaction with Histone-Mimic Nanoparticles through All-Atom Molecular Dynamics. *ACS Nano* **2015**, *9*, 12374−12382.
(24) Ficici, E.; Andricioaei, J. On the Possibility of Facilitated Diffusion of Dendrimers Along DNA. *J. Phys. Chem. B* **2015**, *119*, 6894−6904.
(25) Mondal, S.; Bandyopadhyay, S. Flexibility of the Binding Regions of a Protein−DNA Complex and the Structure and Ordering of Interfacial Water. *J. Chem. Inf. Model* **2019**, *59*, 4427−4437.
(26) Hognon, C.; Garaude, S.; Timmins, J.; Chipot, C.; Dehez, F.; Monari, A. Molecular Bases of DNA Packaging in Bacteria Revealed by All-Atom Molecular Dynamics Simulations: the Case of Histone-Like Proteins in Borrelia Burgdorferi. *J. Phys. Chem. Lett.* **2019**, *10*, 7200−7207.
(27) Materese, C. K.; Savelyev, A.; Papoian, G. A. Counterion Atmosphere and Hydration Patterns near a Nucleosome Core Particle. *J. Am. Chem. Soc.* **2009**, *131*, 15005−15013.
(28) Chakraborty, K.; Kang, M.; Loverde, S. M. Molecular Mechanism for the Role of the H2A and H2B Histone Tails in Nucleosome Repositioning. *J. Phys. Chem. B* **2018**, *122*, 11827−11840.
(29) Winogradoff, D.; Aksimentiev, A. Molecular Mechanism of Spontaneous Nucleosome Unraveling. *J. Mol. Biol.* **2019**, *431*, 323−335.
(30) Matoušková, E.; Bignon, E.; Claerbout, V. E. P.; Dršata, T.; Gillet, N.; Monari, A.; Dumont, E.; Lankaš, F. Impact of the Nucleosome Histone Core on the Structure and Dynamics of DNA-Containing Pyrimidine−Pyrimidone (6−4) Photoproduct. *J. Chem. Theory Comput.* **2020**, *16*, 5972−5981.
(31) Czapla, L.; Swigon, D.; Olson, W. K. Effects of the Nucleoid Protein HU on the Structure, Flexibility, and Ring-Closure Properties of DNA Deduced from Monte Carlo Simulations. *J. Mol. Biol.* **2008**, *382*, 353−370.
(32) Givaty, O.; Levy, Y. Protein Sliding Along DNA: Dynamics and Structural Characterization. *J. Mol. Biol.* **2009**, *385*, 1087−1098.
(33) Korolev, N.; Allahverdi, A.; Yang, Y.; Fan, Y.; Lyubartsev, A. P.; Nordenskiöld, L. Electrostatic Origin of Salt-Induced Nucleosome Array Compaction. *Biophys. J.* **2010**, *99*, 1896−1905.
(34) Cao, Q.; Zuo, C.; Ma, Y.; Li, L.; Zhang, Z. Interaction of Double-Stranded DNA with a Nanosphere: a Coarse-Grained Molecular Dynamics Simulation Study. *Soft Matter* **2011**, *7*, 506−514.
(35) Jiang, Y.; Zhang, D.; Zhang, Y.; Deng, Z.; Zhang, L. The Adsorption-Desorption Transition of Double-Stranded DNA Interacting with an Oppositely Charged Dendrimer Induced by Multivalent Anions. *J. Chem. Phys.* **2014**, *140*, No. 204912.
(36) Chai, A.; Jiang, Y.; Zhang, Y.; He, L.; Zhang, D.; Zhang, L. Wrapping/Unwrapping Transition of Double-Stranded DNA in DNA-Nanosphere Complexes Induced by Multivalent Anions. *Soft Matter* **2014**, *10*, 4875−4884.
(37) Ando, T.; Skolnick, J. Sliding of Proteins Non-specifically Bound to DNA: Brownian Dynamics Studies with Coarse-Grained Protein and DNA Models. *PLoS Comput. Biol.* **2014**, *10*, No. e1003990.
(38) Kenzaki, H.; Takada, S. Partial Unwrapping and Histone Tail Dynamics in Nucleosome Revealed by Coarse-Grained Molecular Simulations. *PLoS Comput. Biol.* **2015**, *11*, No. e1004443.
(39) Park, S.; Joo, H.; Kim, J. S. Directional Rolling of Positively Charged Nanoparticles Along a Flexibility Gradient on Long DNA Molecules. *Soft Matter* **2018**, *14*, 817−825.
(40) Knotts, T. A., IV; Rathore, N.; Schwartz, D. C.; de Pablo, J. J. A Coarse Grain Model for DNA. *J. Chem. Phys.* **2007**, *126*, No. 084901.
(41) Savelyev, A.; Papoian, G. A. Molecular Renormalization Group Coarse-Graining of Polymer Chains: Application to Double-Stranded DNA. *Biophys. J.* **2009**, *96*, 4044−4052.

https://doi.org/10.1021/acsomega.1c01709
ACS Omega 2021, 6, 18728−18736

(42) Ouldridge, T. E.; Louis, A. A.; Doye, J. P. K. Structural, Mechanical, and Thermodynamic Properties of a Coarse-Grained DNA model. *J. Chem. Phys.* **2011**, *134*, No. 085101.
(43) Uusitalo, J. J.; Ingólfsson, H. I.; Akhshi, P.; Tieleman, D. P.; Marrink, S. J. Martini Coarse-Grained Force Field: Extension to DNA. *J. Chem. Theory Comput.* **2015**, *11*, 3932−3945.
(44) Brandner, A.; Schüller, A.; Melo, F.; Pantano, S. Exploring DNA Dynamics within Oligonucleosomes with Coarse-Grained Simulations: SIRAH Force Field Extension for Protein-DNA Complexes. *Biochem. Biophys. Res. Commun.* **2018**, *498*, 319−326.
(45) Chakraborty, D.; Horio, N.; Thirumalai, D. Sequence-Dependent Three Interaction Site Model for Single- and Double-Stranded DNA. *J. Chem. Theory Comput.* **2018**, *14*, 3763−3779.
(46) Humphrey, W.; Dalke, A.; Schulten, K. VMD: Visual Molecular Dynamics. *J. Mol. Graphics* **1996**, *14*, 33−38.
(47) Marrink, S. J.; Risselada, H. J.; Yefimov, S.; Tieleman, D. P.; de Vries, A. H. The MARTINI Force Field: Coarse Grained Model for Biomolecular Simulations. *J. Phys. Chem. B* **2007**, *111*, 7812−7824.
(48) Lin, J.; Zhang, H.; Chen, Z.; Zheng, Y. Penetration of Lipid Membranes by Gold Nanoparticles: Insights into Cellular Uptake, Cytotoxicity, and Their Relationship. *ACS Nano* **2010**, *4*, 5421−5429.
(49) Case, D.; Betz, R.; Cerutti, D.; Cheatham, T., III; Darden, T.; Duke, R.; Giese, T.; Gohlke, H.; Goetz, A.; Homeyer, N. et al. *AMBER 16*; University of California: San Francisco, 2016.
(50) It is Noted That the Exclusion Option Generated by the Script Only Includes Atomic Index of A Single Strand. The Exclusion Option for the Second Strand Is Added Manually in Our Simulations. http://cgmartini.nl/index.php/tutorials-general-introduction-gmx5. Last accessed on 06/23/21.
(51) Mar, W.; Klein, M. L. Molecular Dynamics Study of the Self-Assembled Monolayer Composed of $S(CH_2)_{14}CH_3$ Molecules Using an All-Atoms Model. *Langmuir* **1994**, *10*, 188−196.
(52) Abraham, M. J.; Murtola, T.; Schulz, R.; Páll, S.; Smith, J. C.; Hess, B.; Lindahl, E. GROMACS: High Performance Molecular Simulations through Multi-Level Parallelism from Laptops to Supercomputers. *SoftwareX* **2015**, *1-2*, 19−25.
(53) de Jong, D. H.; Baoukina, S.; Ingólfsson, H. I.; Marrink, S. J. Martini Straight: Boosting Performance Using a Shorter Cutoff and GPUs. *Comput. Phys. Commun.* **2016**, *199*, 1−7.
(54) Parameters for Non-bonded Interactions as Provided in the Tutorial Website of Martini CG Model of DNA. http://www.cgmartini.nl/index.php/tutorials-general-introduction-gmx5. Last accessed on 06/23/21.
(55) Manning, G. Limiting Laws and Counterion Condensation in Polyelectrolyte Solutions I. Colligative Properties. *J. Chem. Phys.* **1969**, *51*, 924−933.
(56) Bloomfield, V. A. Condensation of DNA by Multivalent Cations: Consideration on Mechanism. *Biopolymers* **1991**, *31*, 1471−1481.
(57) Stevens, M. J. Simple Simulations of DNA Condensation. *Biophys. J.* **2001**, *80*, 130−139.
(58) Kosikov, K. M.; Gorin, A. A.; Lu, X.-J.; Olson, W. K.; Manning, G. S. Bending of DNA by Asymmetric Charge Neutralization: All-Atom Energy Simulations. *J. Am. Chem. Soc.*. **2002**, *124*, 4838−4847.
(59) Okonogi, T. M.; Alley, S. C.; Harwood, E. A.; Hopkins, P. B.; Robinson, B. H. Phosphate backbone neutralization increases duplex DNA flexibility: A model for protein binding. *Proc. Natl. Acad. Sci. U.S.A.* **2002**, *99*, 4156−4160.
(60) Xiao, S.; Zhu, H.; Wang, L.; Liang, H. DNA conformational flexibility study using phosphate backbone neutralization model. *Soft Matter* **2014**, *10*, 1045−1055.
(61) Gorman, J.; Greene, E. C. Visualizing One-dimensional Diffusion of Proteins along DNA. *Nat. Struct. Mol. Biol.* **2008**, *15*, 768−774.
(62) Berry, R. S.; Rice, S. A.; Ross, J. *Matter in Equilibrium: Statistical Mechanics and Thermodynamics*, 2nd ed.; Oxford University Press: New York, 2002.

https://doi.org/10.1021/acsomega.1c01709
ACS Omega 2021, 6, 18728−18736